Research Article

eurasia

A Fast Screen System for Dementia Based on EEG Signals

Article History
Received: 19-Dec-2024
Revised: 20-Jan-2025
Accepted: 05-March-2025
Published: 29-March-2025

Norden E. Huang[1,2,3], Wei-Shuai Yuan[1], Fang Yuan[4], Xiao-Min Guo[5], Albert C Yang[3], Terry BJ Kuo[3], TieMei Zhang[6], Jian-Ping Cai[6], Helen Kang[7], Ying-Qiang Zhang[8], Wei-Kuang Liang[2,*]

Abstract: We proposed a set of quantitative, inexpensive, and non-invasive methods for screening dementia based on resting EEG. The methods used here included ensemble Holo spectrum (eHolo), ensemble intrinsic Probability Density function (eiPDF), and ensemble intrinsic Multiscale Entropy (eiMSE). These methods were developed originally for physical sciences, specifically to study the wave-turbulence interaction phenomena. Applications, however, were found in neuroscience and bioengineering. Tested on mostly retrospective open-source EEG data, the results measured by receiver operating characteristic (ROC) curves and area under the curve (AUC) values based on micro- and macro-average methods all passed the clinically acceptable threshold of 70%. Specifically, the AUC scores are these: eHolo above 0.89, eiPDF at 0.82, and eiMSE above 0.87, respectively. If we use all three methods in combination, the AUC score is above 0.91. Emulating the bone-density measurement, we have also established a quantitative Z-score to measure the relative standing of each subject. Encouragingly, the Z-score shows a moderate correlation with the widely scattered CDR score, with RHO values between 0.26 and 0.46. We strongly suggest that large-scale clinical trials be organized so that the method can be validated and ready for the WHO and Chinese calls for screening of the general population by 2030.
Keywords: Fast screening for dementia, eHolo, eiPDF, eiMSE, Holo-Hilbert spectral analysis, Hilbert-Huang Transform.

[1] First Institute of Oceanography, MNR, Qingdao, P. R. China
[2] Institute of Cognitive Neuroscience, National Central University, Zhongli District, Taoyuan City, China
[3] Institute of Brain Science, Brain Research Center, National Yang Ming Chiao Tung University, Taipei, China
[4] Department of health care/gerontology, Qilu Hospital of Shandong University (Qingdao), Qingdao, China
[5] Department of Neurology, The People's Hospital of Shaanxi Province, Xi'an, China
[6] Beijing Hospital, Ministry of Health, Beijing, China
[7] Program in Computational and Systems Biology, MIT, Cambridge, MA, USA
[8] School of Mathematical Sciences, Ocean University of China, Qingdao, China

Co-first authors: Norden E. Huang and Wei-Shuai Yuan:

* **Corresponding Author's Email:** weikuangliang@gmail.com

1. INTRODUCTION

Dementia is a time bomb for any society, rich or poor. With the economic development and the advances of medical and health technology, the worldwide average life expectancy is at a venerable 73.33 years in 2024. But there is another number, the Healthy Life Expectancy (HALE), which varies significantly across different regions. For example, the U.S. had a life expectancy of 78.5 but a HALE of 66.1 years in 2019. During the unhealthy period, dementia is one of the most terrible and costly scourges. To call the attention of the worldwide governments, the World Health Organization, United Nations, issued a plan and call for action in 2017 [1], urging each country to screen at least 50% of their senior citizens for dementia by 2025.

Few countries heeded the call. With 30 percent of the global total dementia sufferers, the Chinese government picked up the challenge and published an action plan and planned to establish a dementia/alzheimer's prevention system by 2030 [2, 3]. However, it is realized that achieving the goal using existing methods and available resources will be extremely challenging. For example, accommodating 50% of the elderly in care institutions would require a cumulative number of 15 million trained dementia care personnel by 2030. Such difficulties had been foreseen by and reported in the World Alzheimer Report 2021 and

2022 [4, 5], and in China by Xiao et al. and Liu et al. [2, 6]. Not only is there a shortage of personnel, but there is also a lack of universal access to the extensive equipment necessary for traditional screening and diagnosis.

The traditional clinical assessment of cognitively challenged patients, as detailed in the *World Alzheimer's Report 2021: Journey through the diagnosis of dementia* [4], is based on primary care providers, or family doctors, who are familiar with the patients. The multiple and varied etiologies of dementia pose a challenge for any attempt to diagnose it. According to the World Alzheimer's Report, dementia could be roughly divided into the following etiologies:

Alzheimer's: 60 to 80%
Vascular dementia: 5 to 10%
Dementia with Lewy bodies:
Frontotemporal dementia
Young-onset dementia: 3%
Mixed dementia

The detailed differential diagnosis was reported by Rosa-Neto [7]. The purpose of the assessment is to identify functional cognition deficits involving learning and memory, language, executive function, complex attention, perceptual-motor, social cognition, and behavior that would impact the patient's autonomy and independence. The key is to identify the presence of disease pathophysiology with biomarkers, with emphasis on Alzheimer's disease (AD). Although AD accounts for only 60–80% of dementia, the separation of AD from the dementia population would influence treatment and care forms. Current dementia diagnosis heavily relies on clinical assessments involving primary care providers and specialists, who evaluate cognitive function primarily through behavioral observations and subjective reporting [4, 5]. However, these traditional methods face numerous limitations. Firstly, they are highly subjective and dependent on clinician expertise and patient cooperation, often resulting in significant misdiagnosis or underdiagnosis rates [4]. Secondly, the clinical assessments are time-consuming, costly, and require substantial medical resources, making large-scale, population-wide screening difficult [2, 6]. Furthermore, many dementia cases involve mixed neuropathologies, complicating accurate diagnosis [8–11]. Granted that there is no cure for the neurodegenerative type of dementia, an earlier diagnosis is urgent, for it could lead to early intervention that might be able to slow down the development of the disease.

Previous EEG-based research has shown the possibility of differentiating dementia patients from healthy controls [e.g., 12–16]. Some prominent electrophysiological features for dementia have been identified, such as "EEG slowing" indexes [see 12], and the decreased theta connectivity [e.g., 14]. We also have demonstrated that by applying a new method, the ensemble intrinsic probability density function (eiPDF) [17], consciousness vs. unconsciousness, different states of sleep, and dementia vs. healthy could be clearly separated by EEG signals. Here we propose two advanced EEG analyses for dementia screening: the ensemble Holo spectrum (eHolo) and the ensemble intrinsic multiscale entropy (eiMSE). These methods collectively allow rapid screening—within approximately 15 minutes—meeting the practical requirements for widespread population screening.

2. METHODS AND MATERIALS

2.1. Basic Requirements of EEG Acquisition and Preprocessing

Basically, even if there are simply two EEG channels, the proposed eiPDF, eHolo, and eiMSE methods can be applied to the EEG signals. However, to obtain the whole brain EEG features based on the three proposed methods, at least the standard 10-20 system with 21 EEG channels is suggested. The sampling rate of data acquisition should be at least 200 Hz to involve gamma oscillations. For obtaining stable results, a minimum of a 3-minute eye-closed resting EEG is required. In addition, employing a preprocessing step of an ICA analysis for the removal of ocular artifacts is preferable.

2.2. Data Sources

The data we used in this study cover a wide range of sources, from the Max-Planck Institute to the local Qingdao Elderly Mental State Cohort, for a total of 1252 subjects, including 772 healthy controls (HC), 207 with mild cognitive impairment (MCI), and 273 with dementia of mixed etiology. The data sources and the demographic information are given in

Table 1 (for open or free data sources, see [18–20]). The local data offered by Qilu Hospital and Shaanxi Provincial People's Hospital were collected through experimental procedures approved by the Institutional Review Board of Qilu Hospital and Shaanxi Provincial People's Hospital, respectively. Furthermore, informed consent was obtained from every subject. For those open data sources, we have confirmed that all the required ethical considerations have been well addressed in the related papers [18–20]. In the following analyses of using each of the three methods, as well as combining all of them, to classify dementia and HC, we limit subjects' ages within the range of 60–100, resulting in 246 dementia and 442 HC. However, when we introduce the use of the Z-score of each feature for estimating each subject's current status, we use all the HC (N_h = 722), a portion of MCI (N_m = 144), and a part of dementia (N_d = 48) to form a reference group similar to the world standard population in which the percentages of HC, MCI, and dementia are approximately 85%, 15%, and 5%.

As the EEG data are from various sources with different EEG systems and montages, these data are pre-processed with the following steps:

1. Based on the standard 10-20 EEG montage, brain waves on 19 channels shared by all the data sources are chosen for the following analysis.
2. The data are resampled at 200 Hz.
3. All data are filtered with a high-pass of 0.5 Hz and a low-pass of 70 Hz, and notch filtered both at 50 and 60 Hz to remove possible power line contamination.
4. Using 3-sigma mean filter to remove outliers.
5. Using Second Order Blind Identification (SOBI) for ICA analysis to remove ocular artifacts [21].
6. Using the Multiple Artifact Rejection Algorithm (MARA) to remove false signals [22, 23].
7. EEG data of bad channels are replaced by interpolation from the neighboring EEG data.
8. Whole brain average-reference is used.

Basically, our preprocessing steps follow the HAPPE program proposed by Gabard-Durnam [24].

2.3. Intrinsic Probability Density Function

In the current study, for each subject, 3 epochs of 50-second EEG are used for the intrinsic probability density function (iPDF) analysis.

The iPDF, as a new way to look at probability density functions (PDF), is proposed by Huang et al. recently [17, 25]. Essentially, iPDF endows the PDF with a spectral-like property that enables us to examine the intrinsic probabilistic properties in great detail for both large and small amplitude components, and stationary and nonstationary processes.

The proposed iPDF is based on Empirical Mode Decomposition (EMD) [26], an adaptive approach designed to analyze data from nonlinear and nonstationary processes. With EMD, any data can be decomposed into a set of intrinsic mode functions (IMFs) that represent oscillatory activities from small to large time scales (see Equation S1). EMD could be viewed as a multi-scale detrending tool [27]. With the EMD expansion, we can study the probability distribution of each intrinsic and scale-separated component, i.e., an IMF, as well as of any partial sum of a range of IMFs for any data, stationary or nonstationary, and gain new physical understanding of the underlying distribution properties. The concrete steps are as follows: First, we will obtain the various partial sums of the IMFs from the data through EMD (see Equation S2), which is essentially an EMD-based high-pass filter bank to detrend the data at various time scales. Since each IMF is zero mean and narrow band, the partial sums should also be zero mean and provide excellent characteristics for being represented as PDFs. The time scale of each partial sum is limited by the last IMF included; thus, the mean period of the last IMF can serve as an estimate of the partial sum's time scale. Next, we will acquire the PDF of each of the partial sums. These PDFs of successive partial sums can be plotted together by representing the probability distributions as a function of time scale and standard deviation. This spectral representation of PDFs in two dimensions could show the clear range of time scales for each underlying PDF pattern in the data. Thus, iPDF is a scale-dependent PDF, whereas traditional PDF is the final marginal result of the full data. To make the results easy to interpret, we employ the PDF of the standard normal distribution as the baseline, i.e., we subtract the standard normal distribution's PDF from the PDF of each partial sum. The resulting baseline-corrected PDFs in various time scales are designated as the intrinsic Probability Density Function (iPDF). The new presentation endows the iPDF as a 'spectrum' like PDF; it is equivalent to a spectrum of PDF, rather than depending solely on z values in a histogram. To increase the stability of the results, we also use a two-layer ensemble approach with different levels of added noise in the data analysis. That is, our iPDF result is an ensemble mean of iPDFs obtained from multiple ensemble EMD (EEMD) [28], with various levels of assisted white Gaussian noise (WGN). We designate the iPDF result as ensemble iPDF (eiPDF).

Table 1: Data sources. OpenneuroCC0: https://doi.org/10.3390/data8060095; MPI: https://doi.org/10.1038/sdata.2018.308; CAUEEG: https://doi.org/10.1016/j.neuroimage.2023.120054; TDBRAIN: https://doi.org/10.1016/j.neuroimage.2023.120054.

		Number				Age							
Dataset's Name	**Clinical Diagnosis**	**Total**	**Female**	**Male**	**Sex n/a**	**Mean**	**Std**	**Min**	**Max**	**Data From**	**Channels**	**Condition**	**Equipment**
QILU(QD)	Healthy Control (MMSE ≥ 27)	178	105	73	0	67.9	5	60	79	Qilu Hospital of Shandong University (Qingdao)	32	Resting EC	ANT32
SXPH	Dementia (CSVD)	32	10	22	0	67	7.3	52	79	Shaanxi People's Hospital	19	Resting EC	SOLAR2848B
	Healthy Control	23	14	9	0	62.7	6	50	79				
AIDI&SSU	Healthy Control	99	32	67	0	21.8	5.7	11	36	AIDI&Shenyang Sport University	32	Resting EC	ANT32
openneuroCC0	Dementia (AD&FTD)	59	33	26	0	65.3	8.1	44	79		19	Resting EC	unknown
	Healthy Control	29	11	18	0	67.9	5.4	57	78				
MPI	Healthy Control	144	50	94	0	39.6	20.5	20	80		62	Resting EC	BP62
CAUEEG	Dementia	182	0	0	182	75.5	8.1	54	94		19	Resting EC	Comet AS40 amplifier
	MCI	207	0	0	207	73.1	8.8	50	93				
	Healthy Control	252	0	0	252	64.8	9.6	23	88				
TDBRAIN	Healthy Control	47	31	16	0	32.2	13.7	18.3	77.4		19	Resting EC	Neuroscan
Total	Total	1252	286	325	641	61	19.4	11	94				
	Dementia	273	43	48	182	72.3	9.2	44	94				
	MCI	207	0	0	207	73.1	8.8	50	93				
	Healthy Control	772	243	277	252	53.6	20.5	11	88				

Additionally, the partial sum distribution would eventually approach the traditional PDF with the full data, which is just the marginal value of the partial sum. Therefore, the partial sum is easily appreciated by and related to the traditional probability study.

It should be pointed out that there is a drastic difference in PDF between additive and multiplicative processes. Linear additive processes are simply superpositions without any interactions between the wave and the white noise. The influence of the dominant wave will only show up when the scale reaches the wave period and leave all the other IMFs untouched. The multiplicative process, however, will influence all the IMF components and make the iPDF super-Gaussian. It should be emphasized that the super-Gaussian characteristics of a PDF should be one of the hallmarks of nonlinear processes.

2.4. The Holo-Hilbert Spectral Analysis and Various Projections

In the current study, for each subject, 10 epochs of 10-second EEG are used for Holo-Hilbert spectral analysis (HHSA) [29].

HHSA is one of the final goals for Hilbert-Huang Transform (HHT) [26]. As designated by NASA, the US Space Agency, the HHT consists of the special adaptive EMD and the spectral representation for nonlinear and nonstationary data. In its final form, HHSA is a multi-dimensional manifold for full representation of time domain data from both additive and multiplicative processes, or for oscillations as well as modulations. Based on HHT, HHSA is also an adaptive method and is designed for nonlinear and nonstationary data.

The HHT is essentially different from the Fourier transform (together with its inverse transform), which is an integral transform that decomposes the time domain data into a linear combination of oscillatory components, each with a constant frequency, ω_j, and a constant amplitude, a_j, resulting in the Fourier spectrum, $F(\omega)$.

In contrast, HHT is achieved by EMD that decomposes any time domain data into IMFs, followed by a process of estimating each IMF's instantaneous frequency and amplitude function through Hilbert transform or an improved direct quadrature method [30], which can be represented as a function of time and the instantaneous frequency, $H(\omega, t)$, referred to as Hilbert time-frequency Spectrum (see Equation S3), or simply Hilbert Spectral Analysis (HSA) [30].

Heavily influenced by the Fourier analysis in the past, HSA had also emphasized the carrier oscillation of the system; therefore, the characteristics of amplitude variation, especially the periodic modulation, are not fully included. To remedy this deficiency, Huang et al. proposed the Holo-Hilbert Spectral analysis (HHSA) by adding a simultaneous expansion of the amplitude achieved by EMD or EEMD [29], designated as the second-layer EMD, which results in the second-layer IMFs, and thus introduces the concept of *amplitude modulation* (AM) and the definition of AM frequency Ω (see Equations S4 & S5). Therefore, the oscillatory power can be represented as a high-dimesional petrum, $HH(\Omega; \omega, t)$, achieved by representing the spectral power on a space spanned by time and the two frequencies, Ω for the amplitude modulation (AM) and ω for the carrier oscillation (or frequency modulation; FM), designated as the Time-FM-AM spectrum of HHSA.

Or, for the sake of ease in presentation, by taking the marginal mean concerning time, we would get a dimensionality-reduced spectrum, which is simply a function of the AM frequency Ω and the carrier frequency ω, referred to as the FM-AM spectrum of HHSA, $HH(\Omega, \omega)$ (see Equation S6). We employ this FM-AM spectrum to demonstrate the results of HHSA in the current study. Similar to eiPDF, our result is an ensemble mean of FM-AM spectra acquired from multiple two-layer EEMD with various levels of assisted WGN. This spectrum is referred to as the ensemble Holo spectrum (eHolo).

2.5. Intrinsic Multiscale Entropy

In the current study, for each subject, 3 epochs of 50-second EEG are used for the intrinsic multiscale entropy analysis. Entropy is an excellent tool to study the brain. It provides a sensitive way of categorizing different groups based on neural functions [31]. Various measures of entropy have been used in analyzing a wide range of biological signals such as in anesthesia (e.g., [32–34]); in aging and degenerative brain (e.g., [35–40]; and review studies: [41, 42]); and in sleep (e.g., [43–45]). Most of the time, these entropy measures provide a holistic measure of the complexity of the system rather than the details of the mechanisms. Furthermore, the results are dif-

ficult to interpret, especially when it comes to relating to the physiological mechanism, partly due to the various approximations made in implementing the computations [46].

Traditionally, entropy is a single value representing the degree of randomness in the data. Costa et al. introduced an approach to analyzing entropy in multiple time scales: the multiscale entropy (MSE) [47, 48], which will give a set of entropy values representing the complexity of the given data in various time scales. This extension greatly expanded the information contained in the results. However, all measures of entropy computation depend on the probability distribution of the data. Therefore, as discussed above (see "**Intrinsic Probability Density Function**"), the MSE cannot escape its limitation to stationary processes. To circumvent the difficulty and also expand the information within the result, Yeh et al. proposed the intrinsic multiscale entropy (iMSE) [49], which computes the MSE consecutively for the partial sums of IMFs, as did the iPDF (see Equation S2). Thus, the entropy result is changed from a single value to a function of time-scale in MSE, and finally to a function of both time-scale and the partial sum's range of IMFs in iMSE. To make the results more stable, similar to eiPDF, our iMSE result is an ensemble mean of iMSEs acquired from multiple EEMD with various levels of assisted WGN. This method is called ensemble iMSE (eiMSE).

3. CLASSIFICATION WORKFLOW

The classification targets are dementia (246 cases) as the positive class, and HC (442 cases) as the negative class. In this study, the special nonlinear features for classifying dementia and HC are extracted from eHolo, eiPDF, and eiMSE, with noise ensembles of added noise levels ranging from 0.01 to 0.07 with a step of 0.01. For each subject, the eHolo is obtained by averaging across eHolo results of 10 epochs of 10-sec eye-closed resting EEG, and the eiPDF or eiMSE is attained by averaging across eiPDF/eiMSE of 3 epochs of 50-sec eye-closed resting EEG. Based on the 19 channels shared by all the data sources, the eHolo, eiPDF, or eiMSE results are further averaged over channels within each of the frontal (F), central (C), parietal and occipital (PO), left temporal (TL), and right temporal (TR) regions to form the regional features (for the information about which region each EEG channel belongs to, please see the following results of data classification using each method). An input feature for each of the three methods is described as follows:

eHolo: The eHolo mean value inside a designated region (F, C, PO, TL, or TR) within a specific dyadic range of AM frequencies (1/8–1/4 Hz, 1/4–1/2 Hz, …, 32–64 Hz; refer to Figs. **1(c, d)** and within a particular dyadic range of FM frequencies (1/4–1/2 Hz, 1/2–1 Hz, …, 32–64 Hz). This yields a total of 220 features (5 regions and 44 AM-FM ranges).

eiPDF: The eiPDF mean value inside a specified region (F, C, PO, TL, or TR) for a particular z value range (one from 4:1:4 ± 0.5) and a certain partial sum (made up of IMFs 1 through n, $n \leq 8$). This gives a total of 360 features (5 regions, 8 partial sums, and 9 z ranges).

eiMSE: The eiMSE mean value inside a designated region (F, C, PO, TL, or TR) for a particular scale (one from [1, 3, 5, 7, 9, 12, 15, 18, 21, 24, 28, 32, 40, 50]) and a certain partial sum (made up of IMFs 1 through n, $n \leq 8$). This results in a total of 560 features (5 regions, 8 partial sums, and 14 MSE scales).

Combined features: Merging all the above feature sets (220 + 360 + 560) gives the entire 1,140 features.

The classifier employed in the current study is Light Gradient-Boosting Machine (LightGBM) [50], applied to each of the four feature scenarios. In each run of LightGBM analysis, random grouping of subjects is performed such that 80% individuals are assigned to the training set and 20% individuals to the testing set. The classification is iterated 25 times to reduce randomness from single runs. For each iteration, the SHAP (SHapley Additive exPlanations) [51] values are computed for all features to quantify each feature's importance. SHAP values from all 25 iterations are further averaged to determine an estimate of the importance of each feature. To preserve critical features while mitigating overfitting risks from high-dimensional data, we perform a procedure of feature selection and optimization in which we retain the top 30% of features based on SHAP values, and then repeat the aforementioned process of iterated classification with the reduced feature set. After that, we calculate the Receiver Operating Characteristic (ROC) curves by aggregating the binary classification probabilities predicted from the 25 iterations. We compute four types of ROC curves:

1) Micro-Average ROC (micro-ROC);
2) Macro-Average ROC (macro-ROC);
3) Dementia-Class ROC (Dementia-ROC); and
4) Healthy Control ROC (HC-ROC).

Figure 1. eHolo results from dementia patients and healthy controls. (a and b) eHolo for dementia patients and healthy controls (HC), respectively. Results from 4 channels (Fp1, Fp2, O1, and O2) are demonstrated. (c) *P* values and (d) *T* map of topographical differences in eHolo between dementia and HC (two-sample *t*-tests). (e) A scheme for classifying dementia and HC achieved by eHolo features designed by a combination of eHolo values from 5 regions of channels, 9 dyadic ranges of AM frequency from 1/8 to 64 Hz, and 8 dyadic ranges of FM frequency from 1/4 to 64 Hz. Four types of ROC curves are shown: 1) Micro-average ROC curve (AUC score: .90)—merge all true positives (TP), false positives (FP), true negatives (TN), and false negatives (FN) in both the dementia and HC classes, and uniformly calculate the global true positive rate (TPR) and false positive rate (FPR); 2) Macro-average ROC curve (AUC score: .89)—calculate TPR and FPR from each class, and then the TPR and FPR are averaged across the two classes; 3) ROC curve of class-1-Dementia (AUC score: .89)—calculate TPR and FPR from the dementia class; and 4) ROC curve of class-2-HC (AUC score: .89)—calculate TPR and FPR from the HC class. (f) The SHAP (SHapley Additive exPlanations) information for the data classification using eHolo.

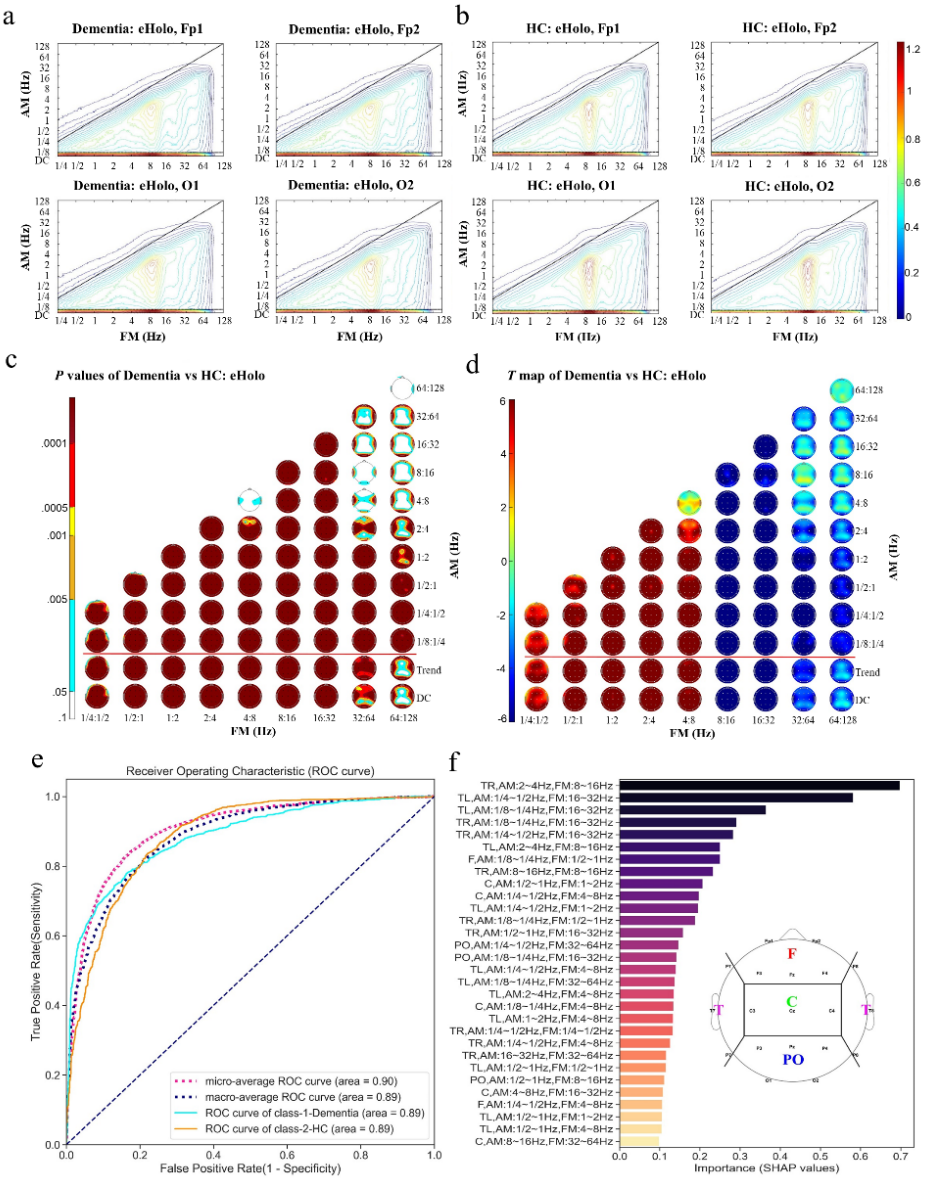

Furthermore, to preserve critical features while mitigating overfitting risks from high-dimensional data, we perform a procedure of feature selection and optimization in which we retain the top 30% of features based on SHAP values, and repeat the process of classification with the reduced feature set. Finally, by aggregating all predictions and comparing them with ground truth labels, we compute the scores of true positive (TP), false negative (FN), false positive (FP), and true negative (TN), thereby obtaining a confusion matrix for the following metrics:

1) Accuracy = (TP + TN) / (TP + FN + TN + FP);
2) Precision = TP / (TP + FP);
3) Sensitivity = TP / (TP + FN);
4) Specificity = TN / (TN + FP); and
5) F1-Score = 2 × Precision × Sensitivity / (Precision + Sensitivity).

4. RESULTS

Having presented the methodologies and data, we are ready to present the results. We first demonstrate the results of eHolo, eiPDF, and eiMSE separately, and then the results of a combination of all three methods.

The presentation format is always on group average from HC and dementia patients with a single electrode measured at frontal (Fp1 and Fp2) and occipital (O1 and O2), based on the standard 10-20 19-channel EEG montage. Then, we will present the group mean topographic maps from all 19 electrodes. The differences of the topographic maps between HC and dementia are given in *P*-values and true magnitudes. Finally, for each method or the combination of the three methods, we present the result of the classification between dementia and HC with ROC curves and AUC scores.

4.1. Holo-Hilbert Spectral Analysis: eHOLO

Figs **1(a, b)** give the group averages of the eHolo spectrum for dementia and HC at Fp1, Fp2, O1, and O2. In both cases, the most energetic components are from the frequency band around 8 Hz, the typical traditional α-band for eye-closed. The differences are clearly visible. Then, the detailed differences for all 19 channels are given in their *P*-values and true magnitude differences, as shown in Fig. **1(c, d)**, respectively. Fig. **1c** indicates that the differences in almost every FM-AM frequency band were statistically significant, and Fig. **1d** indicates that dementia patients suffer a deficiency at high FM frequency bands (8 Hz to 64 Hz) and a surplus at lower FM frequency bands (any bands less than 4 Hz) in spectral power. This trend has been observed by a number of prior studies (e.g., [52–59]).

Finally, Fig. **1e** gives the ROC curve and the AUC score based on micro- and macro-average methods; the values are all at and above 0.89, indicating that using HHSA alone, we can sort out healthy and dementia patients clinically with excellent results. In case clinicians are interested in the location of biomarkers associated with cortical zones to point out the etiology from this machine learning model, the SHAP information [51] is given in Fig. **1f**, in which AM 2 to 4 Hz and FM 8–16 Hz in the TR region is the most important eHolo feature for classifying dementia and HC.

4.2. eiPDF

eiPDF is a newly developed method. Its performance is outstanding in differentiating between consciousness and unconsciousness, as in anesthesia [17]. In the current study, eiPDF is demonstrated for z values from −4 to 4 and for partial sums made up of IMFs 1 through *n*, with all $n \leq 8$. Figs. **2(a, b)** give the group average eiPDF results for HC and dementia at Fp1, Fp2, O1, and O2 electrodes. Again, the differences are visible. The detailed differences from the topographic map based on eiPDF for all 19 channels are given in their *P*-values and true magnitude differences, as shown in Figs. **2(c, d)**, respectively. Here, the statistically significant area is not as solid as in the case of HHSA. Fig. **2d** indicates that dementia patients suffer a deficiency along the mean value of the probability density at z near zero. This implies that the inter-cortical interactions are weaker for the dementia patients than for the healthy control group, which makes the kurtosis value slightly lower. The critical areas seem to concentrate around sigma equals plus and minus 1.

Figure 2. eiPDF results from dementia patients and healthy controls. (a and b) eiPDF for dementia patients and HC. Results from 4 channels (Fp1, Fp2, O1, and O2) are demonstrated. (c) *P* values and (d) *T* map of topographical differences in eiPDF between dementia and HC (two-sample *t*-tests). (e) A scheme for classifying dementia and HC achieved by eiPDF features designed by a combination of eiPDF values from 5 regions of channels, 9 z value ranges from −4 to 4, and 8 partial sums formed by IMFs 1–8. Four types of ROC curves are shown: 1) Micro-average ROC curve (AUC score: .84); 2) Macro-average ROC curve (AUC score: .82); 3) ROC curve of class-1-Dementia (AUC score: .82); and 4) ROC curve of class-2-HC (AUC score: .82). (f) The SHAP information for the data classification through eiPDF. Conventions are the same as in Figure 1.

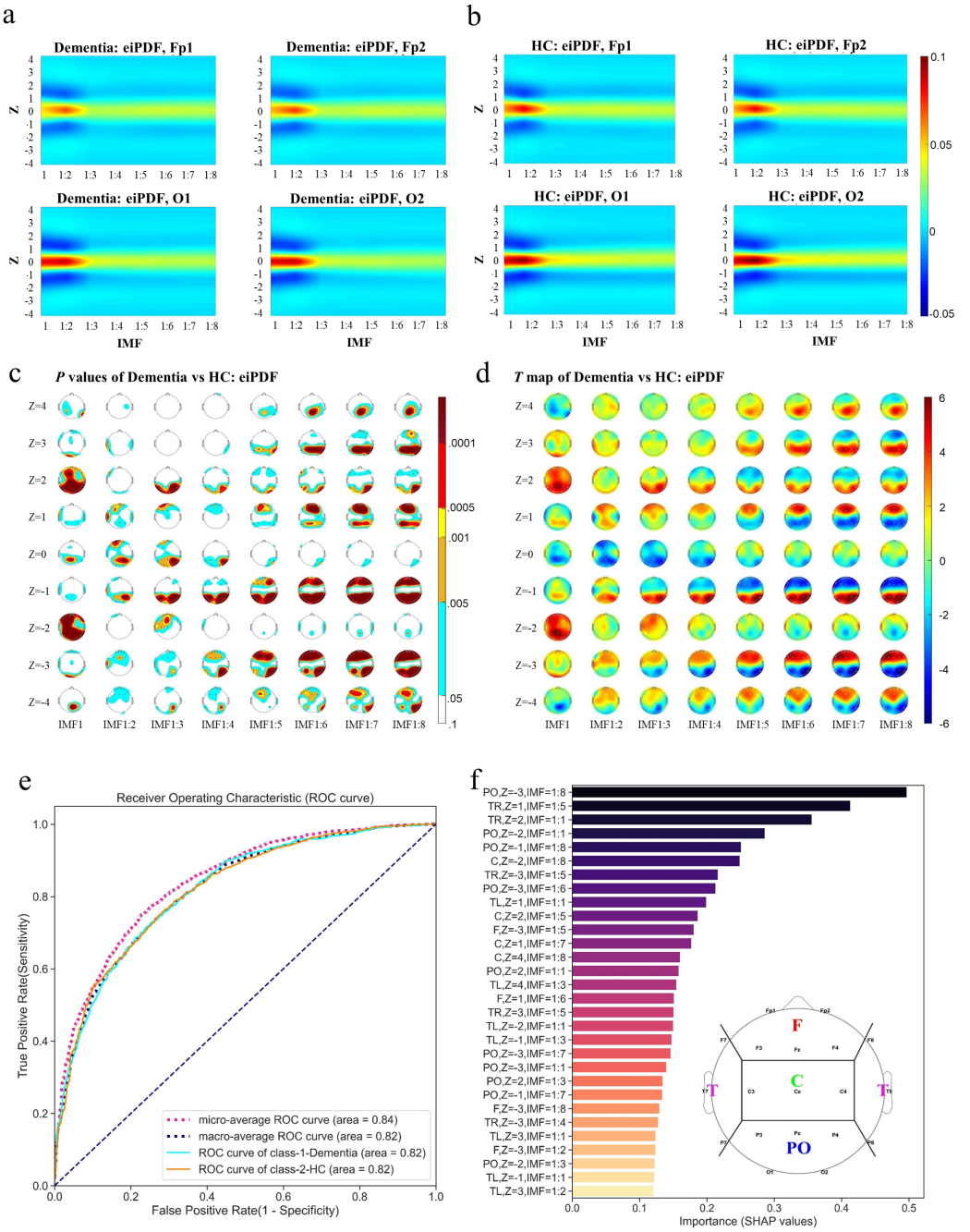

The performance of eiPDF can be seen from the ROC (Receiver Operating Characteristic) curve and the AUC score based on micro- and macro-average methods, given in Fig. **2e**. The scores are at or above 0.82, indicating a good performance but not as satisfactory as the result of eHolo. The SHAP information is given in Fig. **2f**, in which the eiPDF value of the partial sum of IMFs 1:8 and $Z = -3$ in the PO region is the most important eiPDF feature for classifying dementia and HC. As compared to eHolo, eiPDF is easier to compute, and the physiological implications are more direct and clearer: less kurtosis due to fewer modulations from the inter-cortical interactions.

Figure 3. eiMSE results from dementia patients and healthy controls. (a and b) eiMSE for dementia patients and HC. Results from 4 channels (Fp1, Fp2, O1, and O2) are demonstrated. (c) *P* values and (d) *T* map of topographical differences in eiMSE between dementia and HC (two-sample *t*-tests). (e) A scheme for classifying dementia and HC achieved by eiMSE features designed by a combination of eiMSE values from 5 regions of channels, 14 MSE scales: [1, 3, 5, 7, 9, 12, 15, 18, 21, 24, 28, 32, 40, 50], and 8 partial sums formed by IMFs 1–8. Four types of ROC curves are shown: 1) Micro-average ROC curve (AUC score: .90); 2) Macro-average ROC curve (AUC score: .87); 3) ROC curve of class-1-Dementia (AUC score: .87); and 4) ROC curve of class-2-HC (AUC score: .87). (f) The SHAP information for the data classification through eiMSE. Conventions are the same as in Figure 1.

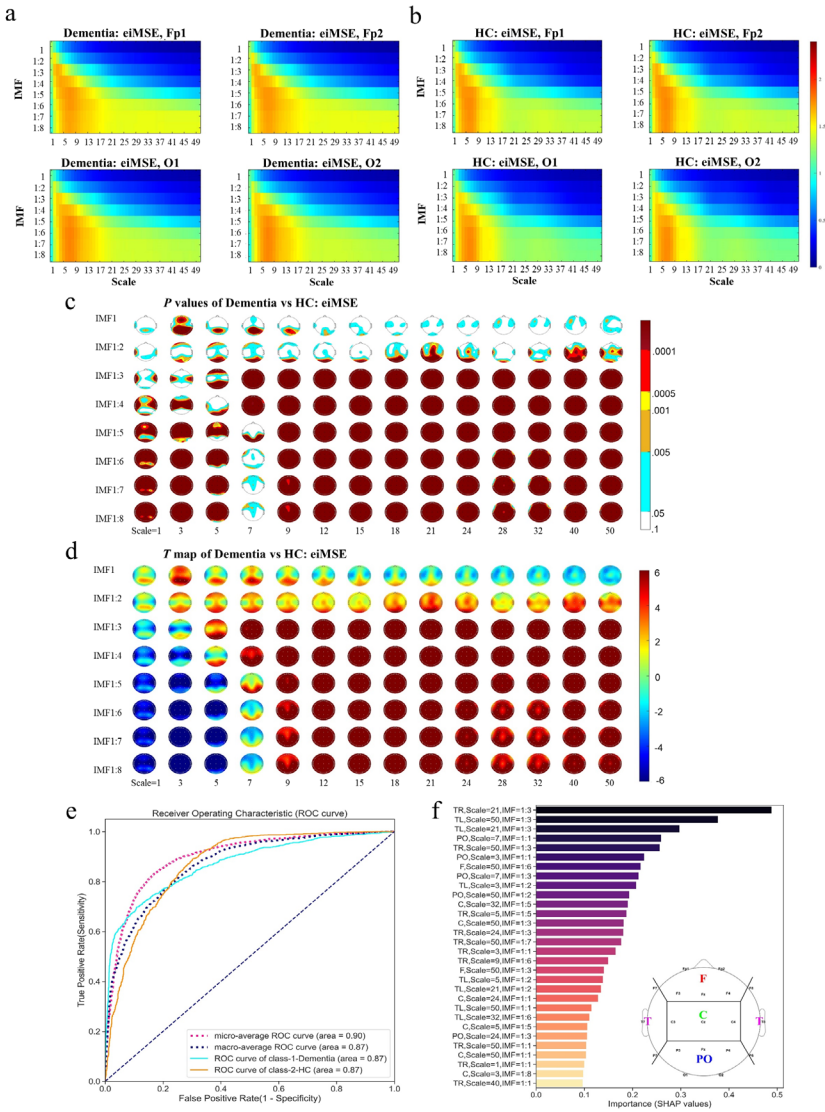

 https://doi.org/10.37819/hb.1.2068

4.3. eiMSE

Usually, eiMSE is more powerful than eHolo and eiPDF for data classification. Figs **3a, b** give the group averages of eiMSE for dementia and HC at Fp1, Fp2, O1, and O2. In this study, eiMSE is computed for scales from 1 to 50, with the MSE parameters m = 2 and r = 0.2, and for partial sums comprising IMFs 1 through n with all $n \leq 8$. This is because we consider the 8th IMF's residue (activity < 0.5 Hz) as the definitive trend of the current investigation. In Figs. **3a and b**, the traditional sample entropy is given by the single value at the lower left corner on scale 1 and the partial sum of IMFs 1:8. The conventional MSE result is given at the margin along the partial sum of IMFs 1:8 with all the scales. The scale information is expanded in eiMSE with the help of EEMD, realizing a systematic detrending process for computing MSE. The transition for the small scales, approximately from 3 to 8, occurs at partial sums of IMFs 1:3 and 1:4 (corresponding to the traditional β and α bands). An energetic component with the scales from 5 to 8 came in the partial sum of IMFs 1:5 and dominated thereafter.

The difference of the 19-channel complexity topographic map is given in Figs. **3(c, d)** for P-values and true magnitude differences. The most statistically significant differences are found around IMF 3 and 4, indicating that the dementia patients suffer a deficiency of entropy at short scales but a surplus of entropy at longer scales, as shown in Fig. **3d.**

Finally, Fig. **3e** gives the ROC (Receiver Operating Characteristic) curve and the AUC score based on micro- and macro-average methods; the values are all at and above 0.87. Thus, we can use eiMSE to sort out healthy and dementia patients clinically with excellent results. In case clinicians are interested in the location of biomarkers associated with cortical zones to explain the etiology from this machine learning model, the SHAP information is given in Fig. **3f**, in which the eiMSE of the partial sum of IMFs 1:3 and scale 21 in the TR region demonstrates the highest importance (i.e., the highest SHAP value) in classifying dementia and HC.

4.4. Full Combination

Having examined each method separately, we can also combine all the methods and give the best result from all the methods. The ROC curve and the AUC score based on micro- and macro-average methods are given in Fig. **4a**. The values are all at and above 0.88, similar to but higher than the results from only eHolo or eiMSE. For clinicians interested in the location of biomarkers associated with cortical zones to point out the etiology from this machine learning model, the SHAP information is given in Fig. **4b**, in which TR FM 8–16 Hz and AM 2–4 Hz, TL FM 16–32 Hz and AM 1/4–1/2 Hz in HHSA, and PO IMF 1:1 and Z = 2 in iPDF show the top three importance in classifying dementia and HC.

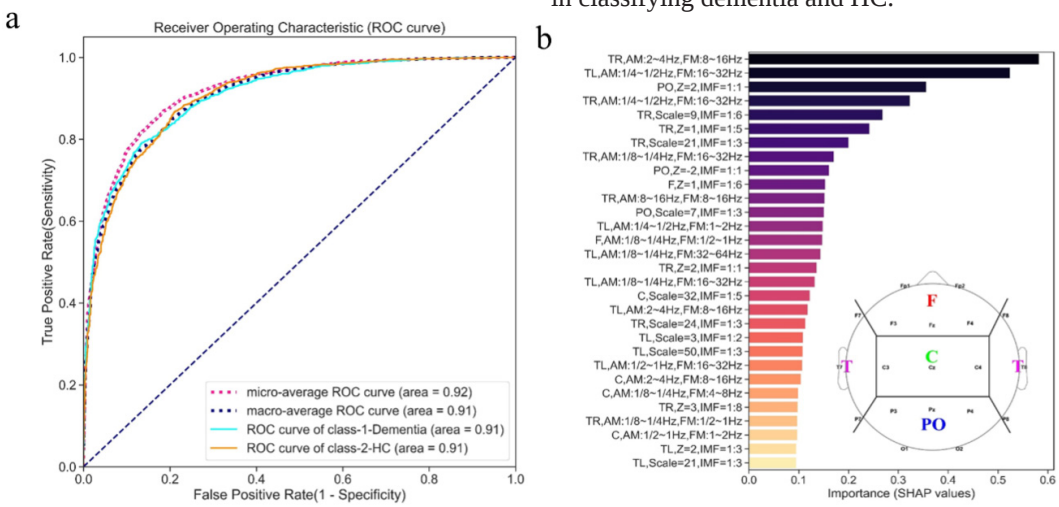

Figure 4. Full combination results for classifying dementia patients and healthy controls. (a) A scheme for classifying dementia and HC by combining eHolo, eiPDF, and eiMSE features. Four types of ROC curves are shown: 1) Micro-average ROC curve (AUC score: .92); 2) Macro-average ROC curve (AUC score: .91); 3) ROC curve of class-1-Dementia (AUC score: .91); and 4) ROC curve of class-2-HC (AUC score: .91). (b) The SHAP information for the data classification through combining features from the three methods. Conventions are the same as in Figure 1.

4.5. Sensitivity and Specificity

Finally, a bar chart (Fig. 5) provides a summary of the performances of each method and their combination for comparison. The eiPDF gives the lowest performance score in every performance index. In general, the combination of all methods outperforms the individual ones, as expected. Based on the AUC scores, all methods could be demonstrated as excellent (eHolo: 0.89; eiPDF: 0.82; eiMSE: 0.87; full: 0.91) in classifying healthy control and dementia. However, these methods show a characteristic of low sensitivity (eHolo: 0.70; eiPDF: 0.57; eiMSE: 0.67; full: 0.70) and high specificity (eHolo: 0.90; eiPDF: 0.87; eiMSE: 0.91; full: 0.92). According to an acceptable standard of clinical testing in which the sum of sensitivity and specificity should be at least 1.5, eHolo (1.6), eiMSE (1.58), and the full combination (1.62) are considered useful, whereas eiPDF (1.44) is not good enough. Nevertheless, considering the computational cost, the direct connection to the modulation, and the visible kurtosis as an indicator, we deem the eiPDF worthy of being included. Appendix 1 demonstrates the confusion matrix of these scores given by the current application of lightGBM to the proposed methods.

Figure 5. A summary of the performances of each method and their combination. Based on the AUC scores, all methods could be demonstrated as excellent (eHolo: 0.89; eiPDF: 0.82; eiMSE: 0.87; full: 0.91) in classifying healthy control and dementia. However, these methods show a characteristic of low sensitivity (eHolo: 0.70; eiPDF: 0.57; eiMSE: 0.67; full: 0.70) and high specificity (eHolo: 0.90; eiPDF: 0.87; eiMSE: 0.91; full: 0.92). According to an acceptable standard of clinical testing in which the sum of sensitivity and specificity should be at least 1.5, eHolo (0.70 + 0.90 = 1.6), eiMSE (0.67 + 0.91 = 1.58), and the full combination (0.70 + 0.92 = 1.62) are considered useful, whereas eiPDF (0.57 + 0.87 = 1.44) is not good enough.

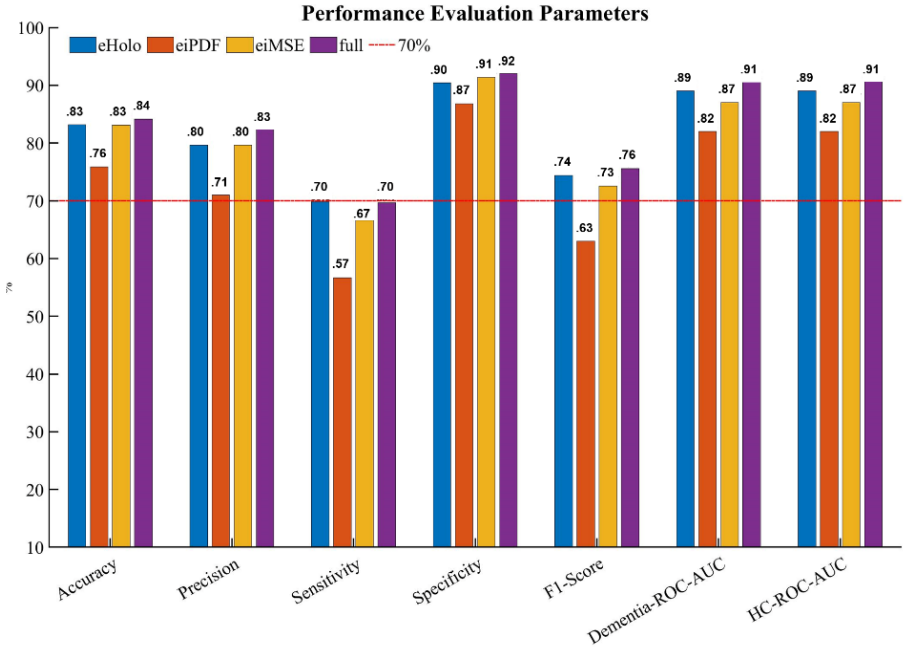

4.6. The Z-Score

Inspired by the bone density measurement, we decided to introduce an overall Z-score, which would be convenient for the patients as well as the health care providers. To calculate the Z-score, we use a reference group (N = 964) that is consistent with the world standard population [60] in the proportions of HC (80%; N_h = 772), mild cognitive impairment (MCI; 15%; N_m = 144), and dementia (5%; N_d = 48). We employ the best feature according to the SHAP scores in each of the nonlinear eHolo, eiPDF, and eiMSE methods, as shown in **Figs. 1f, 2f, and 3f**, to test their effectiveness in screening MCI and dementia in the reference group. Based on each feature, the Z-score of each subject in the reference group, as

well as the corresponding degree of dementia (HC = 0; MCI = 1; and Dementia = 2) of each subject, are shown in Fig. **6a**. Fig. **6b** shows the distributions of the values of the best feature in eHolo, eiPDF, and eiMSE for the subgroups HC, MCI, and Dementia, as well as for the entire reference group. They appear to be distinct from each other. Finally, Fig. **6c** gives the corresponding relationship between Z-score and the degree of dementia for the best feature in eHolo, eiPDF, and eiMSE, showing their Spearman's rank correlation coefficients as −.46, −.26, and .45, respectively, with *Ps* < .001 (Bonferroni corrected for the three analyses). Therefore, we are confident that the current method is useful clinically.

Figure 6. The Z-score for HC, MCI, and Dementia in a reference group. (a) The Z-score of each subject in the reference group based on the best feature of each of the eHolo, eiPDF, and eiMSE methods (black line). Each red line indicates the corresponding degree of dementia (HC = 0; MCI = 1; and Dementia = 2) of these subjects in the reference group. (b) The distributions of the values of the best feature in eHolo, eiPDF, and eiMSE for the subgroups HC, MCI, and Dementia, as well as for the entire reference group. (c) The correlation between Z-score and the degree of dementia for the best feature in eHolo (RHO = −.46; $P < .001$), eiPDF (RHO = −.26; $P < .001$), and eiMSE (RHO = .45; $P < .001$), corrected by Bonferroni method.

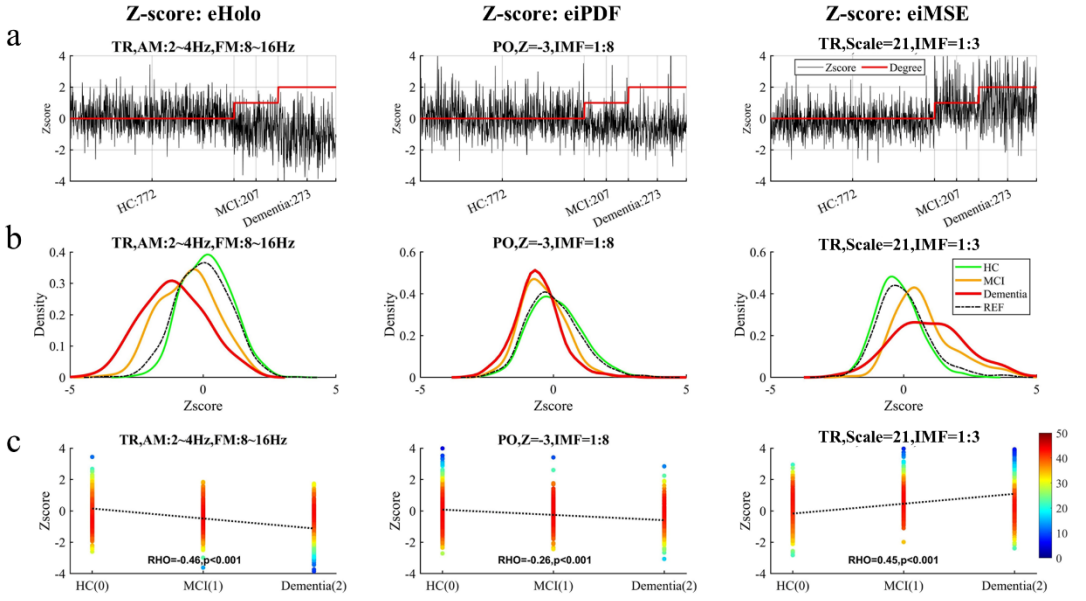

5. DISCUSSION AND CONCLUSION

Based on our analysis, we demonstrate that the nonlinear eHolo, eiPDF, and eiMSE methods are clinically viable for a fast screening of dementia patients, individually or in combination. The administration of these methods is non-invasive, fast, and easy. Fifteen minutes of EEG data acquisition and 10 minutes for off-line analysis would be sufficient for obtaining personalized Z-scores related to classification markers identified by the abovementioned methods. Given that dementia has many different etiologies [7], detecting it must be treated as a first step. A detailed differential diagnosis will have to be followed. The ways to further differentiate the different etiologies using EEG data and nonlinear analysis methods are underway. The preliminary results are encouraging and will be reported separately later.

The differences in eHolo between dementia and HC are closely related to the phenomenon of "EEG slowing", which could potentially be seen in other conditions such as metabolic encephalopathy [e.g., 62]. Therefore, those conditions that share the EEG slowing characteristics may display eHolo patterns similar to dementia. However, since the results of eiPDF and eiMSE are scale-dependent, dementia and other "EEG-slowing" conditions may show different patterns of eiPDF or eiMSE in some scales. Further investigations about whether eHolo, eiPDF, and eiMSE can differentiate dementia from other conditions are needed.

According to the AUC scores, all methods are excellent in classifying healthy controls and dementia. However, our methods in general showed a characteristic of low sensitivity and high specificity. This may be caused by that our data covered a wide range of sources with various EEG montages, amplifiers, and experimental environments. Although trying to limit data sources to a certain montage or amplifier may further improve the performance, the recruitment of a wider range of data sources could be closer to the practical scenario in EEG application.

There are many advantages to using this objective and quantitative method as a screening tool. First, a routine use of this method could provide us with an objective longitudinal standard record for clinic and research purposes. The lack of an objective record has prevented us from being able to forecast the progression of dementia in patients. Second, this fast and quantitative method could help us to fulfill the WHO and the Chinese government's call to screen the elderly population without great trouble. Third, this new method, which focuses on brain function, aims to improve or take the place of the current tests that rely on people's behavior, like the Mini-Mental State Examination (MMSE) and the Montreal Cognitive Assessment (MoCA), which have been shown to be unreliable according to Xiao et al. and Arevalo-Rodriguez et al. [2, 61]. Here, we present an alternative that solely necessitates a basic EEG device, making it portable, affordable, and potentially universally accessible. Following the EEG recording, the fast-screening analysis could be done with a device similar to a sophisticated computer. Thereafter, if the screening result shows that the participant might suffer from dementia, telemetric service could be arranged with real-time results available to the patients and clinicians.

The limitations here are that we have lumped all dementia subtypes together. This is a first step and out of necessity due to the paucity of EEG data collected with other diagnosis methods. Further differential diagnoses are needed and are under development. Most importantly, those patients suffering from Alzheimer's disease need to be further identified as early as possible. As 60–80% of dementia would eventually develop into or be a comorbidity for Alzheimer's, this method could be used as a screening for AD too. We will study those cases as data becomes available. Secondly, given the limited sample size, we should refine the Z-score based on age and sex as the sample size grows. Finally, we demonstrate the current screening method using retrospective data. Although the results are respectable, we should consider organizing and initiating large-scale clinical trials to validate the method so that we can fulfill the WHO and Chinese government calls to screen dementia cases fast and inexpensively by 2030.

Declarations of Interest

The authors have no conflicts of interest.

Funding

This work was supported by the National Science and Technology Council, Taiwan (grant numbers: 113-2410-H-008-071; 111-2410-H-008-044-MY2). A part of the data employed by this study, offered by Qilu Hospital of Shandong University (Qingdao, China), was collected under the support of the QLACS project funded by the Qingdao Health Commission of Laoshan District and the Qingdao Key Health Discipline Development Fund. The Natural Science Foundation of Shandong Province, China (Grant No ZR2017MH124).

References

[1] World Health Organization. Global action plan on the public health response to dementia 2017–2025 [Internet]. Geneva: The World Health Organization; 2017 [cited 2025 Apr 28]. Available from: https://www.who.int/publications/i/item/global-action-plan-on-the-public-health-response-to-dementia-2017---2025

[2] Xiao J, Lia J, Wanga J, Zhangb X, Wang C, Pengd G, et al. Alzheimer's disease facts and figures. *Alzheimers Dement*. 2023;19(4):1598–1695. doi:10.1002/alz.13016

[3] Chinese National Action Plan for Alzheimer's Disease. 应对老年期痴呆国家行动计划 (2024-2030) [Internet]. 2024 [cited 2025 Apr 28]. Available from: http://www.nhc.gov.cn/lljks/tggg/202501/2a01a6e45016496789370a276e8762f0.shtml

[4] Gauthier S, Rosa-Neto P, Morais JA, Webster C. World Alzheimer Report 2021: Journey through the diagnosis of dementia [Internet]. London: Alzheimer's Disease International; 2021 [cited 2025 Apr 28]. Available from: https://

www.alzint.org/resource/world-alzheimer-report-2021

[5] Gauthier S, Webster C, Servaes S, Morais JA, Rosa-Neto P. World Alzheimer Report 2022: Life after diagnosis: Navigating treatment, care and support [Internet]. London: Alzheimer's Disease International; 2022 [cited 2025 Apr 28]. Available from: https://www.alzint.org/u/World-Alzheimer-Report-2022.pdf

[6] Liu Y, et al. Projection for dementia burden in China to 2050: A macro-simulation study by scenarios of dementia incidence trends. *Lancet Reg Health West Pac.* 2024;50:101158. doi:10.1016/j.lanwpc.2021.101158

[7] Rosa-Neto P. Differential diagnosis. In: Gauthier S, Rosa-Neto P, Morais JA, Webster C, editors. World Alzheimer Report 2021: Journey through the diagnosis of dementia. London: Alzheimer's Disease International; 2021. Chapter 14. Available from: https://www.alzint.org/resource/world-alzheimer-report-2021

[8] Brenowitz WD, Hubbard RA, Keene CD, Hawes SE, Longstreth WT Jr, Woltjer RL, et al. Mixed neuropathologies and estimated rates of clinical progression in a large autopsy sample. Alzheimers Dement. 2017;13(6):654–62. doi:10.1016/j.jalz.2016.09.015

[9] Wang X, Zhu K, Wu W, Zhou D, Lu H, Du J, et al. Prevalence of mixed neuropathologies in age-related neurodegenerative diseases: A community-based autopsy study in China. *Alzheimers Dement*. 2025;21(1):e14369. doi:10.1002/alz.14369

[10] Schneider JA, Arvanitakis Z, Bang W, Bennett DA. Mixed brain pathologies account for most dementia cases in community-dwelling older persons. *Neurology*. 2007;69(24):2197–204. doi:10.1212/01.wnl.0000271090.28148.24

[11] Kapasi A, DeCarli C, Schneider JA. Impact of multiple pathologies on the threshold for clinically overt dementia. *Acta Neuropathol.* 2017;134(2):171–86. doi:10.1007/s00401-017-1717-7

[12] Tanaka M, Yamada E, Mori F. Neurophysiological markers of early cognitive decline in older adults: a mini-review of electroencephalography studies for precursors of dementia. *Front Aging Neurosci.* 2024;16:1486481.

[13] Nayana BR, Pavithra MN, Chaitra S, Bhuvana Mohini TN, Stephan T, Mohan V, et al. EEG-based neurodegenerative disease diagnosis: comparative analysis of conventional methods and deep learning models. *Sci Rep.* 2025;15(1):15950.

[14] Chetty CA, Bhardwaj H, Kumar GP, et al. EEG biomarkers in Alzheimer's and prodromal Alzheimer's: a comprehensive analysis of spectral and connectivity features. *Alz Res Therapy*. 2024;16:236. doi:10.1186/s13195-024-01582-w. 2025;Preprint:13872877251327754.

[15] Kopčanová M, Tait L, Donoghue T, Stothart G, Smith L, Flores-Sandoval AA, et al. Resting-state EEG signatures of Alzheimer's disease are driven by periodic but not aperiodic changes. *Neurobiol Dis.* 2024;190:106380.

[16] Hu D, Chen M, Li X, Daley S, Morin P, Han Y, et al. Unlocking the potential of EEG in Alzheimer's disease research. *Clin Neurophysiol.* 2025;136:93–102.

[17] Huang NE, Yuan W, Yang ACC, Kuo TBJ, Tang WX, Kang H, et al. Quantifying consciousness through the intrinsic Probability Density Function. Under Review

[18] Miltiadous A, Tzimourta KD, Afrantou T, Ioannidis P, Grigoriadis N, Tsalikakis DG, et al. A dataset of scalp EEG recordings of Alzheimer's disease, frontotemporal dementia and healthy subjects from routine EEG. *Data*. 2023;8(6):95. doi:10.3390/data8060095

[19] Babayan A, Erbey M, Kumral D, Reinelt JD, Reiter AMF, Röbbig J, et al. A mind-brain-body dataset of MRI, EEG, cognition, emotion, and peripheral physiology in young and old adults. *Sci Data.* 2019;6:180308. doi:10.1038/sdata.2018.308

[20] Kim MJ, Youn YC, Paik J. Deep learning-based EEG analysis to classify normal, mild cognitive impairment, and dementia: Algorithms and dataset. *Neuroimage*. 2023;272:120054. doi:10.1016/j.neuroimage.2023.120054

[21] Fatnan MH, Hussain Z. Blind source separation under semi-white Gaussian noise and uniform noise: Performance analysis of ICA, SOBI, and JadeR. *J Comput Sci*. 2019;15(1):27–44. doi:10.3844/jcssp.2019.27.44

[22] Winkler I, Haufe S, Tangermann M. Automatic classification of artifactual ICA-components for artifact removal in EEG signals. *Behav Brain Funct.* 2011;7(1):30. doi:10.1186/1744-9081-7-30

[23] Winkler I, Brandl S, Horn F, Waldburger E, Allefeld C, Tangermann M. Robust artifactual

independent component classification for BCI practitioners. *J Neural Eng*. 2014;11(3):035013. doi:10.1088/1741-2560/11/3/035013

[24] Gabard-Durnam LJ, Mendez Leal AS, Wilkinson CL, Levin AR. The Harvard Automated Processing Pipeline for Electroencephalography (HAPPE): Standardized processing software for developmental and high-artifact data. *Front Neurosci*. 2018;12:97. doi:10.3389/fnins.2018.00097

[25] Huang NE, Yuan W, Kang X. Monitoring Method and System Based on Intrinsic Probability Density Function. Chinese Patent. 2025.05.27: CN 120036771 A.

[26] Huang NE, Shen Z, Long SR, Wu MC, Shih HH, Zheng Q, et al. The empirical mode decomposition method and the Hilbert spectrum for non-stationary time series analysis. *Proc R Soc Lond A Math Phys Eng Sci*. 1998;454(1971):903–95. doi:10.1098/rspa.1998.0193

[27] Wu Z, Huang NE, Long SR, Peng CK. On the trend, detrending, and variability of nonlinear and nonstationary time series. *Proc Natl Acad Sci U S A*. 2007;104(38):14889–94. doi:10.1073/pnas.0701020104

[28] Wu Z, Huang NE. Ensemble empirical mode decomposition: A noise-assisted data analysis method. *Adv Adapt Data Anal*. 2009;1(1):1–41. doi:10.1142/S1793536909000042

[29] Huang NE, Hu K, Yang ACC, Chang HC, Jia D, Liang WK, et al. On Holo-Hilbert spectral analysis: A full informational spectral representation for nonlinear and non-stationary data. *Philos Trans A Math Phys Eng Sci*. 2016;374(2065):20150206. doi:10.1098/rsta.2015.0206

[30] Huang NE, Wu Z, Long SR, Arnold KC, Chen X, Blank K. On instantaneous frequency. *Adv Adapt Data Anal*. 2009;1(2):177–229. doi:10.1142/S1793536909000096

[31] Keshmiri S. Entropy and the brain: An overview. *Entropy*. 2020;22(9):917. doi:10.3390/e22090917

[32] Shalbaf R, Behnam H, Sleigh JW, Steyn-Ross A, Voss LJ. Monitoring the depth of anesthesia using entropy features and an artificial neural network. *J Neurosci Methods*. 2013;218(1):17–24. doi:10.1016/j.jneumeth.2013.03.008

[33] Su C, Liang Z, Li X, Li D, Li Y, Ursino M. A comparison of multiscale permutation entropy measures in online depth of anesthesia monitoring. *PLoS One*. 2016;11(10):e0164104. doi:10.1371/journal.pone.0164104

[34] Liu Q, Chen YF, Fan SZ, et al. EEG artifacts reduction by multivariate empirical mode decomposition and multiscale entropy for monitoring depth of anaesthesia during surgery. *Med Biol Eng Comput*. 2017;55:1435–50. doi:10.1007/s11517-016-1598-2

[35] Hogan MJ, Kilmartin L, Keane M, et al. Electrophysiological entropy in younger adults, older controls, and older cognitively declined adults. *Brain Res*. 2012;1445:1–10. doi:10.1016/j.brainres.2012.01.028

[36] Schätz M, Vyšata O, Kopal J, Procházka A. Comparison of complexity, entropy and complex noise parameters in EEG for AD diagnosis. *J Neurol Sci*. 2013;333:e355. doi:10.1016/j.jns.2013.07.1303

[37] Houmani N, Dreyfus G, Vialatte FB. Epoch-based entropy for early screening of Alzheimer's disease. *Int J Neural Syst*. 2015;25(4):1550032. doi:10.1142/S0129065715500327

[38] Ruiz-Gómez S, Gómez C, Poza J, Gutiérrez-Tobal G, Tola-Arribas M, Cano M, et al. Automated multiclass classification of spontaneous EEG activity in Alzheimer's disease and mild cognitive impairment. *Entropy*. 2018;20(1):35. doi:10.3390/e20010035

[39] Niu Y, Wang B, Zhou M, et al. Dynamic complexity of spontaneous bold activity in Alzheimer's disease and mild cognitive impairment using multiscale entropy analysis. *Front Neurosci*. 2018;12:677. doi:10.3389/fnins.2018.00677

[40] Şeker M, Özbek Y, Yener G, Özerdem MS. Complexity of EEG dynamics for early diagnosis of Alzheimer's disease using permutation entropy neuromarker. *Comput Methods Programs Biomed*. 2021;206:106116. doi:10.1016/j.cmpb.2021.106116

[41] Ouchani M, Gharibzadeh S, Jamshidi M, Amini M. A review of methods of diagnosis and complexity analysis of Alzheimer's disease using EEG signals. *Biomed Res Int*. 2021;2021:5425569. doi:10.1155/2021/5425569

[42] Aviles M, Sánchez-Reyes LM, Álvarez-Alvarado JM, Rodríguez-Reséndiz J. Machine and deep learning trends in EEG-based detection and diagnosis of Alzheimer's disease: A systematic review. *Eng*. 2024;5(3):1464–84. doi:10.3390/eng5030078

[43] Burioka N, Miyata M, Cornélissen G, Halberg F, Takeshima T, Kaplan DT, et al. Approximate entropy in the electroencephalogram during wake and sleep. *Clin EEG Neurosci*. 2005;36(1):21–4. doi:10.1177/155005940503600106

[44] Shi W, Feng H, Zhang X, Yeh CH. Amplitude modulation multiscale entropy characterizes complexity and brain states. *Chaos Solitons Fractals*. 2023;173:113646. doi:10.1016/j.chaos.2023.113646

[45] Miskovic V, MacDonald KJ, Rhodes LJ, Cote KA. Changes in EEG multiscale entropy and power-law frequency scaling during the human sleep cycle. *Hum Brain Mapp*. 2019;40(2):538–51. doi:10.1002/hbm.24393

[46] Delgado-Bonal A, Marshak A. Approximate entropy and sample entropy: A comprehensive tutorial. *Entropy*. 2019;21(6):541. doi:10.3390/e21060541

[47] Costa M, Goldberger AL, Peng CK. Multiscale entropy analysis of physiologic time series. *Phys Rev Lett*. 2002;89(6):062102. doi:10.1103/PhysRevLett.89.062102

[48] Costa M, Goldberger AL, Peng CK. Multiscale entropy analysis of biological signals. *Phys Rev E*. 2005;71(2):021906. doi:10.1103/PhysRevE.71.021906

[49] Yeh JR, Peng CK, Huang NE. Scale-dependent intrinsic entropies of complex time series. *Philos Trans A Math Phys Eng Sci*. 2016;374(2065):20150204. doi:10.1098/rsta.2015.0204

[50] Ke G, Meng Q, Finley T, Wang T, Chen W, Ma W, et al. LightGBM: A highly efficient gradient boosting decision tree. *Adv Neural Inf Process Syst*. 2017;30.

[51] Lundberg SM, Lee SI. A unified approach to interpreting model predictions. *Adv Neural Inf Process Syst*. 2017;30:4765–74.

[52] Bi X, Wang H. Early Alzheimer's disease diagnosis based on EEG spectral images using deep learning. *Neural Netw*. 2019;114:119–35. doi:10.1016/j.neunet.2019.02.005

[53] Ieracitano C, Mammone N, Bramanti A, Hussain A, Morabito FC. A convolutional neural network approach for classification of dementia stages based on 2D-spectral representation of EEG recordings. *Neurocomputing*. 2019;323:96–107. doi:10.1016/j.neucom.2018.09.071

[54] Ieracitano C, Mammone N, Hussain A, Morabito FC. A novel multi-modal machine learning based approach for automatic classification of EEG recordings in dementia. *Neural Netw*. 2020;123:176–90. doi:10.1016/j.neunet.2019.12.006

[55] Sharma N, Kolekar MH, Jha K, Kumar Y. EEG and cognitive biomarkers based mild cognitive impairment diagnosis. *IRBM*. 2019;40(2):113–21. doi:10.1016/j.irbm.2018.11.007

[56] Zheng X, Wang B, Liu H, Wu W, Sun J, Fang W, et al. Diagnosis of Alzheimer's disease via resting-state EEG: Integration of spectrum, complexity, and synchronization signal features. *Front Aging Neurosci*. 2023;15:1288295. doi:10.3389/fnagi.2023.1288295

[57] Chu KT, Lei WC, Wu MH, Fuh JL, Wang SJ, French IT, et al. A holo-spectral EEG analysis provides an early detection of cognitive decline and predicts the progression to Alzheimer's disease. *Front Aging Neurosci*. 2023;15:1195424. doi:10.3389/fnagi.2023.1195424

[58] Wang R, He Q, Shi L, et al. Automatic detection of Alzheimer's disease from EEG signals using an improved AFS–GA hybrid algorithm. *Cogn Neurodyn*. 2024;18:2993–3013. doi:10.1007/s11571-024-10130-z

[59] Jack CR Jr, Andrews JS, Beach TG, Buracchio T, Dunn B, Graf A, et al. Revised criteria for diagnosis and staging of Alzheimer's disease: Alzheimer's Association Workgroup. *Alzheimers Dement*. 2024;20(8):5143–69. doi:10.1002/alz.13859

[60] United Nations, Department of Economic and Social Affairs, Population Division. World population prospects 2024 [Internet]. 2024 [cited 2025 Apr 28]. Available from: https://population.un.org/wpp/

[61] Arevalo-Rodriguez I, Smailagic N, Roqué-Figuls M, Ciapponi A, Sanchez-Perez E, Giannakou A, et al. Mini-Mental State Examination (MMSE) for the early detection of dementia in people with mild cognitive impairment (MCI). *Cochrane Database Syst Rev*. 2021;7(7):CD010783. doi:10.1002/14651858.CD010783.pub3

[62] Lin CC. EEG manifestations in metabolic encephalopathy. *Acta Neurol Taiwan*. 2005;14(3):151–161.

Appendix 1: Summary of the confusion metrix scores based on lightGBM.

	eHolo	eiPDF	eiMSE	Full
Accuracy	0.83	0.76	0.83	0.84
Precision	0.80	0.71	0.80	0.83
Sensitivity	0.70	0.57	0.67	0.70
Specificity	0.90	0.87	0.91	0.92
F1-Score	0.74	0.63	0.73	0.76